ARTICLE

USP19 suppresses inflammation and promotes M2-like macrophage polarization by manipulating NLRP3 function via autophagy

Tao Liu[1], Liqiu Wang[1], Puping Liang[1], Xiaojuan Wang[2], Yukun Liu[1], Jing Cai[1], Yuanchu She[1], Dan Wang[2], Zhi Wang[3], Zhiyong Guo[4], Samuel Bates[5], Xiaojun Xia[2], Junjiu Huang[1] and Jun Cui[1,2]

Macrophage polarization to proinflammatory M1-like or anti-inflammatory M2-like cells is critical to mount a host defense or repair tissue. The exact molecular mechanisms controlling this process are still elusive. Here, we report that ubiquitin-specific protease 19 (USP19) acts as an anti-inflammatory switch that inhibits inflammatory responses and promotes M2-like macrophage polarization. USP19 inhibited NLRP3 inflammasome activation by increasing autophagy flux and decreasing the generation of mitochondrial reactive oxygen species. In addition, USP19 inhibited the proteasomal degradation of inflammasome-independent NLRP3 by cleaving its polyubiquitin chains. USP19-stabilized NLRP3 promoted M2-like macrophage polarization by direct association with interferon regulatory factor 4, thereby preventing its p62-mediated selective autophagic degradation. Consistent with these observations, compared to wild-type mice, *Usp19*$^{-/-}$ mice had decreased M2-like macrophage polarization and increased interleukin-1β secretion, in response to alum and chitin injections. Thus, we have uncovered an unexpected mechanism by which USP19 switches the proinflammatory function of NLRP3 into an anti-inflammatory function, and suggest that USP19 is a potential therapeutic target for inflammatory interventions.

Keywords: Inflammasome; Autophagy; Macrophage polarization; Deubiquitinating enzyme; NLRP3

Cellular & Molecular Immunology (2021) 18:2431–2442; https://doi.org/10.1038/s41423-020-00567-7

INTRODUCTION

Macrophages are versatile and plastic effector cells of the innate immune system. They are critical for host defense, inflammation resolution, and wound healing.[1] In response to environmental signals, macrophages display a functional spectrum. M1- (proinflammatory) and M2-like (anti-inflammatory) macrophages are the two extremes on this functional spectrum.[2] M1-like macrophages are triggered by the invasion of pathogenic microorganisms, interferon (IFN) gamma and/or Toll-like receptor (TLR) ligands to produce numerous proinflammatory cytokines, including tumor necrosis factor (TNF-α), interleukin (IL)-1β, and IL-6. They promote bacterial killing, phagocytosis, and inflammatory responses.[2] In contrast, M2-like macrophages are activated by IL-4 or IL-13, and express a unique subset of genes, including those that encode inflammatory zone 1 (FIZZ1), chitinase-3-like protein 3 (YM1), IL-10, and mannose receptor (MR).[3] Compared to M1-like macrophages, M2-like macrophages have a decreased ability to present antigens to T cells and produce anti-inflammatory cytokines.[3] To maintain balance between robust anti-pathogen immunity and tissue homeostasis, delicate mechanisms are required to safeguard macrophage polarization.

Various signaling pathways regulate the balance of M1- and M2-like macrophage polarization. For example, the production of IL-1β, a marker for M1-like macrophage polarization, is controlled by multiple steps. First, the activation of nuclear factor kappa B (NF-κB) is required for the transcription of pro-IL-1β and NOD-like receptor family, pyrin domain containing 3 (NLRP3). NLRP3 is then activated in response to various stimuli, leading to the oligomerization of apoptosis-associated speck-like protein containing a CARD (ASC), and the recruitment of pro-caspase-1 for the maturation and release of IL-1β.[4] In contrast, several key transcription factors, including signal transducer and activator of transcription 6 (STAT6), Kruppel-like factor 4 (KLF4), and interferon regulatory factor 4 (IRF4),[5–7] dominate the anti-inflammatory responses of M2-like macrophages. Mechanistic target of rapamycin complex 1 (mTORC1) and mTORC2 also facilitate M2-like macrophage polarization in cooperation with these transcription factors.[8,9] Nonetheless, the exact molecular mechanisms responsible for macrophage polarization remain poorly understood.

Ubiquitin-specific protease 19 (USP19) is an endoplasmic reticulum (ER)-anchored deubiquitinating enzyme that regulates ER-associated protein degradation and DNA damage repair.[10,11]

[1]MOE Key Laboratory of Gene Function and Regulation, State Key Laboratory of Biocontrol, School of Life Sciences, Sun Yat-sen University, 510275 Guangzhou, Guangdong, People's Republic of China; [2]Department of Experimental Medicine, State Key Laboratory of Oncology in South China, Sun Yat-sen University, 510275 Guangzhou, People's Republic of China; [3]Guanghua School of Stomatology, Guangdong Provincial Key Laboratory of Stomatology, Stomatological Hospital, Sun Yat-Sen University, 510060 Guangzhou, Guangdong, People's Republic of China; [4]Organ Transplant Center, The First Affiliated Hospital, Sun Yat-Sen University, 510080 Guangzhou, Guangdong, People's Republic of China and [5]Channing Division of Network Medicine, Brigham and Women's Hospital and Harvard Medical School, Boston, MA 02115, USA
Correspondence: Junjiu Huang (hjunjiu@mail.sysu.edu.cn) or Jun Cui (cuij5@mail.sysu.edu.cn)
These authors contributed equally: Tao Liu, Liqiu Wang, Puping Liang

Received: 22 May 2020 Accepted: 26 September 2020
Published online: 23 October 2020

Recently, emerging evidence has shown that USP19 acts as a crucial negative regulator of the immune response by distinct mechanisms. It directly inhibits TNF-α/IL-1β- and TLR3/4-mediated signaling by deubiquitinating TAK1 and TRIF, respectively.[12,13] Recently, we reported that USP19 stabilizes the Beclin-1 protein to promote autophagy and inhibit type I IFN signaling.[14] Autophagy is closely related to many cellular processes, including host defense and tissue repair.[14] To fully understand the function of USP19 in regulating the crosstalk between autophagy and immune responses in vivo, we generated *USP19*-knockout (KO; *Usp19*$^{-/-}$) mice and found that USP19 inhibited NLRP3 inflammasome activation in M1-like macrophages by promoting autophagy-mediated reactive oxygen species (ROS) clearance. Furthermore, we unexpectedly found that USP19 inhibited p62/SQSTM1 (hereafter referred to as p62)-dependent selective autophagy of IRF4 through NLRP3 deubiquitination, thus promoting M2-like macrophage polarization. Hence, we have identified USP19 as a pivotal anti-inflammatory regulator that switches the proinflammatory function of NLRP3 into an anti-inflammatory function, and suggest that USP19 may serve as a therapeutic target in the prevention and treatment of inflammation-associated diseases.

RESULTS

USP19 deficiency promoted a proinflammatory response in alum-induced peritonitis

We previously showed that USP19 promotes autophagosome formation by stabilizing the Beclin-1 protein (encoded by BECN1).[14] To investigate whether USP19 regulates innate immune responses via autophagy in vivo, we generated conventional KO mice by CRISPR/Cas9 technology. We validated that *Usp19* deficiency decreased Beclin-1 stability in bone marrow (BM) cells (Supplementary Fig. S1a–c). Autophagy was reported to induce the clearance of PAMPs (pathogen-associated molecular patterns) or DAMPs (damage-associated molecular patterns) to attenuate inflammation.[15] To uncover the role of USP19 in inflammation, we used the aluminium salt (hereafter referred to as alum)-induced peritonitis model to detect the production of IL-1β, an inflammatory cytokine involved in inflammation and autoimmune conditions.[16–19] We found that the lavage fluid of *Usp19*$^{-/-}$ mice contained significantly increased concentrations of IL-1β than that of wild-type (WT) mice (Fig. 1a).

To determine whether elevated IL-1β production in *Usp19*$^{-/-}$ mice was associated with increased macrophage recruitment, we quantified macrophages in the lavage fluid. Unexpectedly, the total number of macrophages was decreased in *Usp19*$^{-/-}$ mice upon alum treatment (Fig. 1b, c). We deduced that the balance between M1-like macrophages and M2-like macrophages might be changed in *Usp19*$^{-/-}$ mice. Indeed, we found that the proportion of M2-like macrophages (F4/80^{+}CD11b^{+}MR^{+}; Fig. 1d, e), but not M1-like macrophages (F4/80^{+}CD11b^{+}CD86^{+}; Fig. 1f), was significantly decreased in *Usp19*$^{-/-}$ mice after alum treatment.

Macrophage polarization is closely related to neutrophil and eosinophil recruitment.[20,21] Thus, we quantified neutrophils and eosinophils in peritoneal exudate cells (PECs) and found that alum-induced recruitment of neutrophils (CD11b^{+}Ly6G^{+}) was strongly enhanced in *Usp19*$^{-/-}$ mice compared to WT mice (Fig. 1g, h). In contrast, the recruitment of eosinophils (CD11b^{+}Siglec-F^{+}) was severely impaired in *Usp19*$^{-/-}$ mice (Fig. 1i, j). Therefore, these results demonstrate that *Usp19* deficiency switched anti-inflammatory responses to proinflammatory responses in an alum-induced peritonitis model.

The loss of USP19 enhanced IL-1β secretion by promoting NLRP3 inflammasome activation

Given that USP19 significantly inhibited IL-1β production in an alum-induced peritonitis model, we considered that USP19 might regulate inflammasome activation. We isolated different cell types from *Usp19*$^{-/-}$ mice and examined inflammasome activation. NLRP3 was reported to activate inflammasomes, and the loss of NLRP3 abrogated IL-1β secretion.[22,23] Thus, we treated cells with ATP, alum, and silica to activate NLRP3-mediated IL-1β secretion and found that *Usp19* depletion significantly increased IL-1β release in response to ATP, alum, and silica stimulation in bone-marrow-derived macrophages (BMDMs), bone marrow-derived dendritic cells (BMDCs), and mouse embryonic fibroblasts (MEFs), whereas poly(dA:dT) (an AIM2 inflammasome activator)-induced IL-1β secretion remained largely unaltered (Fig. 2a and Supplementary S2a, b). USP19 has been reported to specifically regulate NF-κB signaling by targeting TLR 3/4 signaling.[12,13] Here, we applied R848 (a TLR7/8 ligand) and PGN (a TLR2 ligand) to our system to induce inflammasome activation,[24–27] and observed that *Usp19* deficiency increased IL-1β production. Thus, in addition to the role of USP19 in TLR3/4 signaling, our data supported the notion that USP19 also targets inflammasome activation and affects inflammatory responses (Supplementary Fig. S2c). In addition, we detected the cleavage of caspase-1 and found increased amounts of cleaved caspase-1 in the supernatant of ATP-treated BMDMs from *Usp19*$^{-/-}$ mice compared to WT mice, indicating that *Usp19* deficiency indeed enhanced NLRP3 inflammasome activation (Fig. 2b–d).

We also confirmed that the loss of *USP19* increased NLRP3 inflammasome activation in human THP-1-derived macrophages. Small interfering RNA (siRNA)-mediated *USP19* silencing resulted in increased IL-1β release in response to NLRP3 inflammasome agonists in lipopolysaccharide (LPS)-primed THP-1-derived macrophages, when compared to scrambled control siRNA-transfected cells (Supplementary Fig. S2d, e). During inflammasome activation, NLRP3 triggers the formation of ASC specks through PYD–PYD-mediated interactions.[28] In *USP19*-KO THP-1 cells, ASC speck formation in LPS-primed and ATP-challenged THP-1-derived macrophages was significantly enhanced in response to the inflammasome activation (Fig. 2e, f and Supplementary S2f). Activated caspase-1 cleaves the gasdermin D protein to drive a form of inflammatory cell death known as pyroptosis.[29] We next assessed the role of USP19 in ATP-, alum-, silica-, and poly(dA:dT)-induced cell death. Upon NLRP3 inflammasome activation, cell death was more prominent in *Usp19*$^{-/-}$ cells than in WT cells, while no difference due to AIM2-mediated inflammasome activation was observed (Fig. 2g). To further confirm that USP19 suppresses NLRP3 inflammasome activation, we used siRNAs to knockdown endogenous *Nlrp3* in WT and *USP19*-KO THP-1-derived macrophages, and found that the depletion of *NLRP3* abrogated IL-1β upregulation in *USP19*-KO cells in response to LPS and ATP (Supplementary Fig. S2g, h). Together, these results indicate that *USP19* deficiency specifically enhances NLRP3 inflammasome activation and cell death.

USP19-mediated autophagy restrains ROS production to inhibit NLRP3 inflammasome activation

ROS are a major signal that activates the NLRP3 inflammasome.[30] To determine whether USP19 affects NLRP3 inflammasome activation via ROS production, we examined ROS accumulation in WT and *Usp19*$^{-/-}$ macrophages, and found that *Usp19* deficiency largely enhanced ROS production (Fig. 2h, i). Furthermore, treatment of macrophages with the mitochondrial-targeted antioxidant Mito-TEMPO, a specific scavenger of mitochondrial ROS,[31] abrogated increased IL-1β secretion in *Usp19*$^{-/-}$ macrophages (Fig. 2j). These data suggest that the depletion of *USP19* enhances NLRP3 inflammasome activation by upregulating mitochondrial ROS production. Previously, we showed that USP19 promotes autophagy via Beclin-1 stabilization.[32] To examine whether USP19-mediated autophagy affects mitochondrial ROS production, we knocked down *Beclin-1* and found that the upregulation of ROS induced by *Usp19* deficiency was diminished in the absence of Beclin-1 (Fig. 2k). Strikingly, the loss

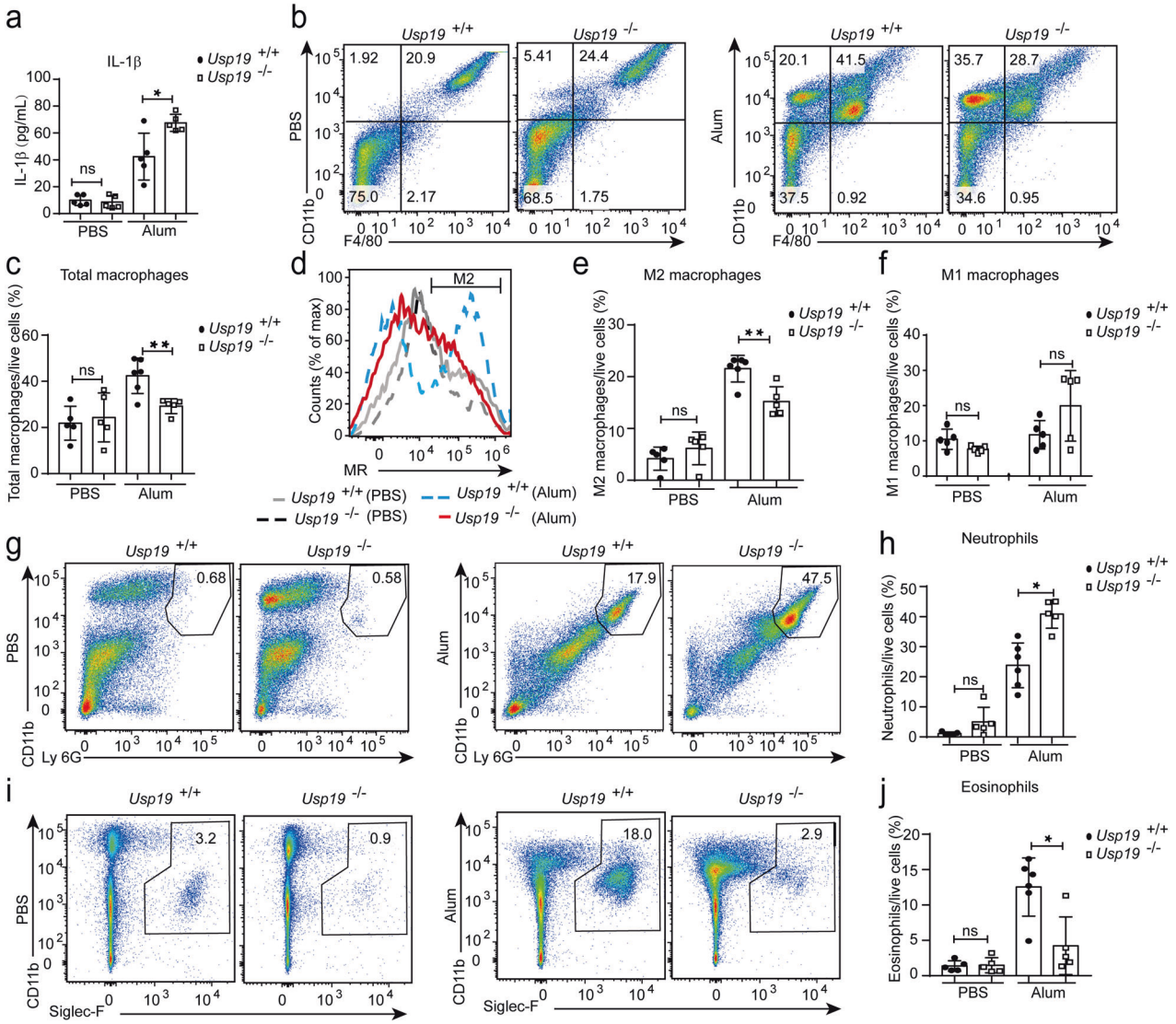

Fig. 1 USP19 deficiency promoted alum-induced peritonitis. **a** ELISA analysis of interleukin (IL)-1β in peritoneal exudate cells (PECs) harvested from wild-type (WT) or *Usp19*$^{-/-}$ mice after intraperitoneal injection (i.p.) with or without alum for 12 h (mice: WT-PBS, $n = 5$; *Usp19*$^{-/-}$-PBS, $n = 5$; WT-alum, $n = 5$; *Usp19*$^{-/-}$-alum, $n = 5$). **b** Expression of CD11b and F4/80 in PECs harvested from alum-treated WT or *Usp19*$^{-/-}$ mice. Quadrants and numbers among an indicated percentage of cells in each gate (F4/80^{+}CD11b^{+}, F4/80^{+}CD11b^{-}, F4/80^{-}CD11b^{+}, and F4/80^{-}CD11b^{-}). **c** Percentage of F4/80^{+}CD11b^{+} macrophages (total macrophages) in PECs harvested from i.p. injected WT or *Usp19*$^{-/-}$ mice (mice: WT-PBS, $n = 5$; *Usp19*$^{-/-}$-PBS, $n = 5$; WT-alum, $n = 6$; *Usp19*$^{-/-}$-alum, $n = 5$). **d** Surface mannose receptor (MR) expression on peritoneal F4/80^{+}CD11b^{+} macrophages from WT or *Usp19*$^{-/-}$ mice with alum stimulation. The graph shows MR expression on macrophages on the horizontal axis. **e** F4/80^{+}CD11b^{+}MR^{+} macrophages (M2-like macrophages) in PECs harvested from WT or *Usp19*$^{-/-}$ mice with alum administration (mice: WT-PBS, $n = 5$; *Usp19*$^{-/-}$-PBS, $n = 5$; WT-alum, $n = 6$; *Usp19*$^{-/-}$-alum, $n = 5$). **f** F4/80^{+}CD11b^{+}CD86^{+} macrophages (M1-like macrophages) among PECs harvested from WT or *Usp19*$^{-/-}$ mice administered alum (mice: WT-PBS, $n = 5$; *Usp19*$^{-/-}$-PBS, $n = 5$; WT-alum, $n = 5$; *Usp19*$^{-/-}$-alum, $n = 5$). **g** Expression of CD11b and Ly6G in PECs harvested from alum-injected WT or *Usp19*$^{-/-}$ mice. Quadrants and numbers among an indicated percentage of cells in each gate (CD11b^{+}Ly6G^{+}, CD11b^{+}Ly6G^{-}, CD11b^{-}Ly6G^{+}, and CD11b^{-}Ly6G^{-}). **h** Percentage of CD11b^{+}Ly6G^{+} (neutrophils) among PECs harvested from alum-treated WT or *Usp19*$^{-/-}$ mice (mice: WT-PBS, $n = 5$; *Usp19*$^{-/-}$-PBS, $n = 5$; WT-alum, $n = 6$; *Usp19*$^{-/-}$-alum, $n = 5$). **i** Expression of CD11b and Siglec-F in PECs from WT or *Usp19*$^{-/-}$ mice injected with alum. Quadrants and numbers among an indicated percentage of cells in each gate (CD11b^{+}Siglec-F^{+}, CD11b^{+}Siglec-F^{-}, CD11b^{-}Siglec-F^{+}, and CD11b^{-}Siglec-F^{-}). **j** Percentage of CD11b^{+}Siglec-F^{+} (eosinophils) among PECs harvested from alum-treated WT or *Usp19*$^{-/-}$ mice (mice: WT-PBS, $n = 5$; *Usp19*$^{-/-}$-PBS, $n = 5$; WT-alum, $n = 5$; *Usp19*$^{-/-}$-alum, $n = 5$). In **a**, **c**, **e**, **f**, **h**, and **j**, data are the mean values ± SDs, ns (nonsignificant), $P > 0.05$; *$P < 0.05$; **$P < 0.01$; ***$P < 0.001$ (Student's *t* test)

of Beclin-1 abrogated the effects of USP19 on IL-1β secretion (Fig. 2l). Taken together, these results suggest that the loss of USP19/Beclin-1 impairs autophagy, leading to the increased ROS production and subsequent NLRP3 inflammasome activation.

Depletion of USP19 impaired M2-like macrophage polarization

IL-4 secreted from basophils, eosinophils, and Th2-type CD4 lymphocytes can promote M2-like macrophage polarization.[33] To determine whether decreased M2-like macrophage polarization in alum-treated *Usp19*$^{-/-}$ mice (Fig. 1d) was intrinsic or due to decreased IL-4 expression from other cells, we treated WT and *Usp19*$^{-/-}$ BM cells with IL-4 and found that expression of the M2-like macrophage-associated markers *Il-10*, *MR*, and *Ym1* was significantly decreased in *Usp19*$^{-/-}$ cells (Fig. 3a), suggesting an intrinsic role for USP19 in promoting M2-like macrophage polarization. Chitin, a widespread environmental biopolymer of

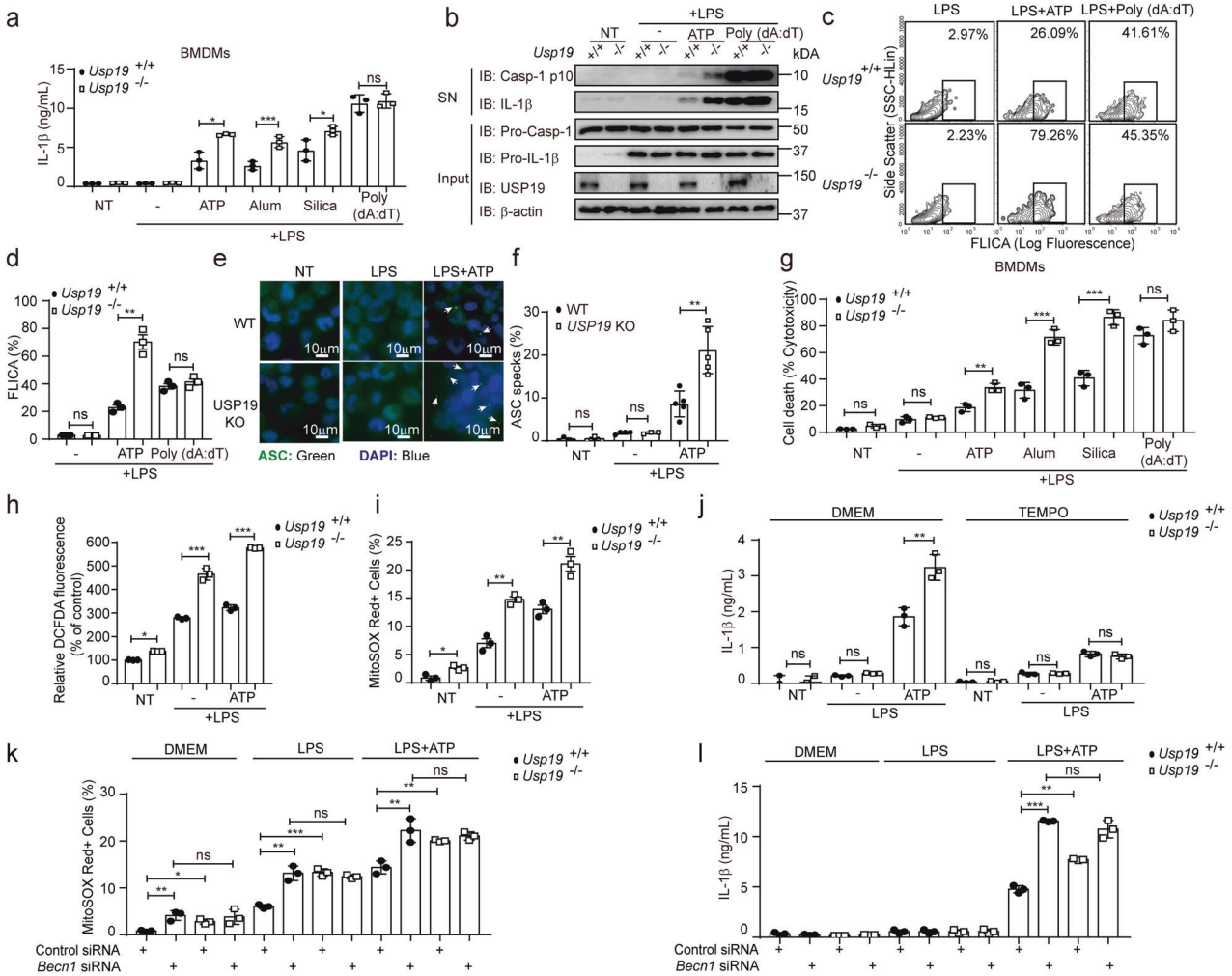

Fig. 2 USP19 promotes autophagy-mediated reactive oxygen species (ROS) clearance to inhibit NLRP3 inflammasome activation. **a** Bone-marrow-derived macrophages (BMDMs) were pretreated in culture medium with LPS (500 ng/mL) for 3 h, followed by ATP (5 mM, 6 h), alum (500 μg/mL, 6 h), silica (500 μg/mL, 6 h), or poly(dA:dT) (2 μg/mL, 6 h) administration. NT untreated. Cell supernatants were collected to measure IL-1β release by ELISA. **b**–**d** BMDMs were treated as in **a**; subsequently, cell lysates and culture supernatants were collected for immunoblot analysis (**b**), or cells were digested for fluorescent-labeled inhibitor of caspases (FLICA) staining (**c**). Quantification of FLICA staining is listed (**d**). **e**, **f** THP-1-derived macrophages from wild-type (WT) or *USP19*-knockout (KO) cell lines primed with or without LPS (100 ng/mL, 3 h) and challenged with ATP (5 mM) for 6 h. ASC foci (green) and DAPI (blue) were detected by immunostaining. Scale bar, 10 μm (**e**). Statistics of the percentages of cells containing ASC foci are listed (**f**). ASC, green; DAPI, blue. **g** WT or *Usp19*$^{-/-}$ BMDMs were treated with the indicated stimuli, and the culture supernatant was then collected to measure cell death by lactate dehydrogenase release. **h** Mitochondrial ROS in WT or *Usp19*$^{-/-}$ BMDMs primed with LPS (500 ng/mL, 3 h) and treated with ATP (5 mM, 6 h), as assessed by the fluorescence of cells stained with 2′,7′-dichlorofluorescein diacetate (DCFDA) using a fluorescence microplate reader (excitation and emission wavelengths of 485 and 538 nm, respectively). ROS generation is presented as the percentage relative to the value in the control culture. **i** WT or *Usp19*$^{-/-}$ BMDMs were transfected with control small interfering RNA (siRNA) or *Becn1* siRNA for 48 h. Cells were stimulated with LPS (500 ng/mL, 3 h), and ROS was assessed by flow cytometry of cells stained with a fluorogenic dye targeted to mitochondria (MitoSOX). **j** WT or *Usp19*$^{-/-}$ BMDMs were preincubated with Mito-TEMPO (500 μM) for 1 h, followed by LPS (500 ng/mL, 3 h) and ATP (5 mM, 6 h) administration. IL-1β secretion was analyzed by ELISA. **k**, **l** WT or *Usp19*$^{-/-}$ BMDMs were transfected with control siRNA or *Becn1* siRNA for 48 h. Cells were stimulated with LPS (500 ng/mL, 3 h), and ROS was assessed by flow cytometry of cells stained with a fluorogenic dye targeted to mitochondrial ROS (**k**), or the cell supernatants were collected to measure IL-1β release by ELISA (**l**). In **a**, **d**, and **f**–**l**, data are the mean values ± SEMs, ns (nonsignificant), $P > 0.05$; *$P < 0.05$; **$P < 0.01$; ***$P < 0.001$ (Student's *t* test). For **a**–**c**, **g**, **j**, and **l**, similar results were obtained from three independent biological experiments

N-acetyl-b-D-glucosamine, is a structural component of helminths, arthropods, and fungi.[34] Chitin administration in the peritoneum can specifically direct M2-like macrophage polarization.[7] Thus, we intraperitoneally injected the mice with chitin and found that the proportion of peritoneal macrophages (Fig. 3b), particularly F4/80^{+}CD11b^{+}MR^{+} macrophages (Fig. 3c), obtained from *Usp19*$^{-/-}$ mice was decreased. Consistent with this observation, we found that mRNA levels of the M2-like macrophage-associated genes *Fizz1* and *MR* in PECs from chitin-treated *Usp19*$^{-/-}$ mice were also decreased (Fig. 3d). In addition, we found that the number of chitin-elicited eosinophils was also decreased in *Usp19*$^{-/-}$ mice (Fig. 3e, f). Together, these results indicate that USP19 is critical to promote M2-like macrophage polarization in response to chitin administration.

USP19 prevents IRF4 from p62-mediated selective autophagic degradation

We next sought to determine whether USP19 promotes M2-like macrophage polarization by acting on the key transcription factors of M2-like macrophages, including IRF4, STAT6, and KLF4.[5–7] We performed a cycloheximide (CHX) "chase" assay and found that *Usp19* deficiency led to the significant degradation of endogenous

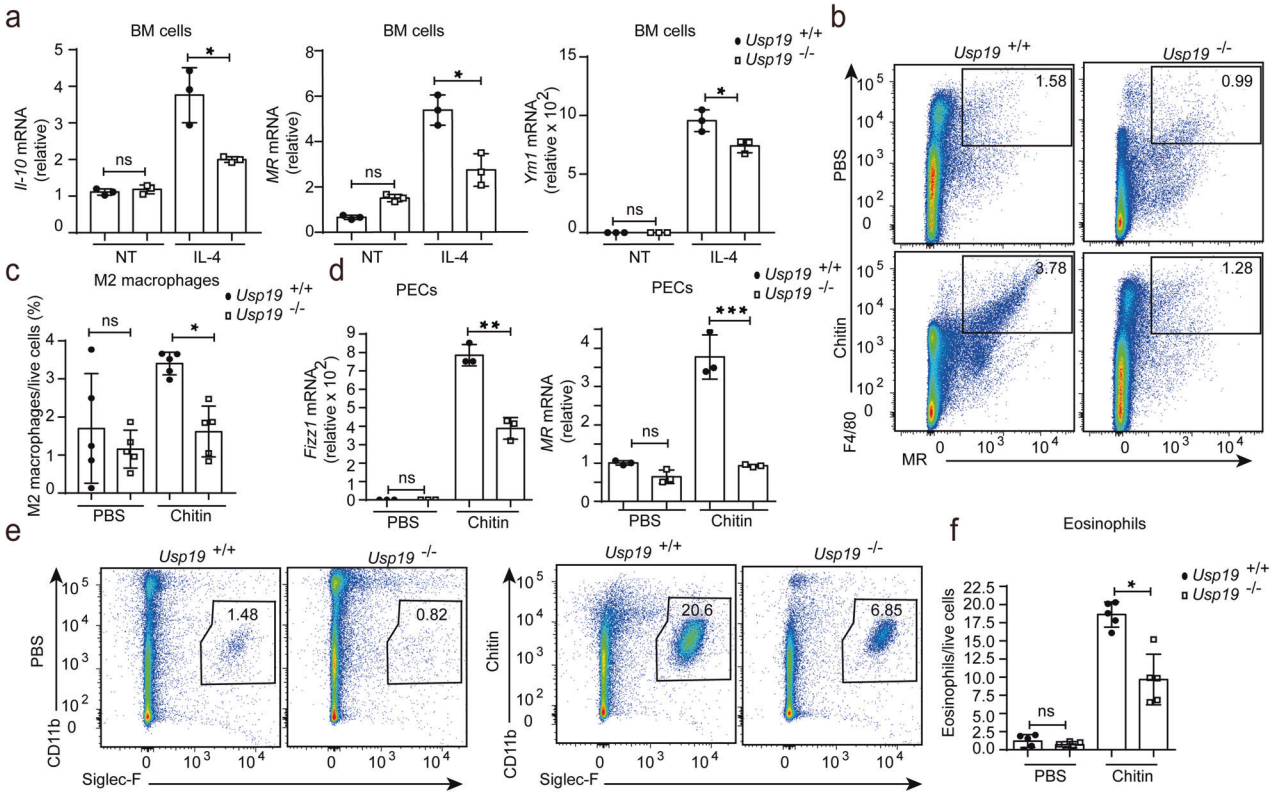

Fig. 3 USP19 is critical for M2-like macrophage polarization. **a** Bone marrow macrophages (BMs) cultured for 24 h in medium alone were treated with IL-4 (20 ng/mL). Total RNA was harvested from the treated cells at 24 h and used for real-time PCR analysis to determine the expression of *Il-10*, *MR*, and chitinase-3-like protein 3 (*Ym1*; relative to *Gapdh*). **b** Expression of MR and F4/80 in PECs harvested from wild-type (WT) or *Usp19*$^{-/-}$ mice injected with chitin. Quadrants and numbers among an indicated percentage of cells in each gate (F4/80^{+}MR^{+}, F4/80^{+}MR^{-}, F4/80^{-}MR^{+}, and F4/80^{-}MR^{-}). **c** Percentage of F4/80^{+}MR^{+} macrophages (M2-like macrophages) among PECs harvested from chitin-treated WT or *Usp19*$^{-/-}$ mice (mice: WT-PBS, $n = 5$; *Usp19*$^{-/-}$-PBS, $n = 5$; WT-chitin, $n = 5$; *Usp19*$^{-/-}$-chitin, $n = 5$). **d** PECs were collected from WT or *Usp19*$^{-/-}$ mice i.p. injected with chitin. Total RNA was harvested from PECs at 48 h and used for real-time PCR analysis to determine the expression of found in inflammatory zone 1 (*Fizz1*) and *MR* (relative to *Gapdh*). **e** Expression of CD11b and Siglec-F in PECs harvested from WT or *Usp19*$^{-/-}$ mice stimulated with chitin. Quadrants and numbers among an indicated percentage of cells in each gate (CD11b^{+}Siglec-F^{+}, CD11b^{+}Siglec-F^{-}, CD11b^{-}Siglec-F^{+}, and CD11b^{-}Siglec-F^{-}). **f** Percentage of CD11b^{+}Siglec-F^{+} (eosinophils) among PECs harvested from chitin-injected WT or *Usp19*$^{-/-}$ mice (mice: WT-PBS, $n = 5$; *Usp19*$^{-/-}$-PBS, $n = 5$; WT-chitin, $n = 5$; *Usp19*$^{-/-}$-chitin, $n = 5$). For **a** and **d**, similar results were obtained from three independent biological experiments. In **c** and **f**, data are the mean values ± SDs, ns (nonsignificant), $P > 0.05$; *$P < 0.05$; **$P < 0.01$; ***$P < 0.001$ (Student's *t* test)

IRF4, but not KLF4 or STAT6 (Fig. 4a). Notably, the rate of IRF4 degradation was accelerated in *Usp19*-deficient cells compared with the WT group. In addition, we did not observe much difference in *Irf4* mRNA levels between WT and *Usp19*-deficient cells (Supplementary Fig. S3a). We next observed that the overexpression of USP19 increased IRF4 protein levels in human embryonic kidney (HEK) 293T cells with stable NLRP3 expression (referred to as HEK293T-NLRP3 cells; Fig. 4b). Given that *IRF4* mRNA was not altered with USP19 overexpression, the increased IRF4 abundance occurred at the protein level (Fig. 4b). To determine which domain of IRF4 was stabilized by USP19, we cotransfected HEK293T-NLRP3 cells with Myc-USP19, and Flag-tagged IRF4 truncated mutants. Immunoblot analysis showed that USP19 stabilized both the C- and N-terminal domains of IRF4 (Supplementary Fig. S3b). Interestingly, we found that USP19-mediated stabilization of IRF4 was completely inhibited by the autophagy inhibitor 3-methyladenine (3-MA), autolysosome inhibitor chloroquine (CQ), or ammonium chloride (NH_4Cl), as well as the proteasome inhibitors MG132, lactacystin, and carfilzomib (Fig. 4c, d). These results demonstrated that USP19 stabilizes IRF4 through blocking either the autolysosome or proteasome pathway. In addition, we subjected BM cells to autophagy-inducing conditions, including starvation and rapamycin treatment, and found that the IRF4 protein level was decreased. In contrast, the inhibitors of autophagy bafilomycin, tubacin, and CQ blocked IRF4 degradation (Supplementary Fig. S3c). Different cargo receptors are known to direct specific target proteins to lysosomes for autophagic degradation.[15] We examined the interactions of IRF4 with different cargo receptors and found that IRF4 specifically interacted with p62, but not Nip3-like protein X (NIX), optineurin (OPTN), neighbor of BRCA1 (NBR1), tollip, or nuclear dot 10 protein 52 (NDP52; Fig. 4e). Further experiments showed that IRF4 did not associate with other key proteins in the autophagy process, including members of the unc-51 like autophagy activating kinase 1 complex, Beclin-1 complex, autophagy-related 5–12 (ATG5-12) or ATG7 (Supplementary Fig. S3d, e). In addition, we found that IRF4 colocalized with LC3B in the presence of NH4Cl (Supplementary Fig. S3f). These data indicate that IRF4 is recruited to autophagosomes through the cargo receptor p62. Further immunoprecipitation analysis showed that the C-terminus of IRF4 is responsible for the IRF4–p62 interaction (Supplementary Fig. S3g). Next, we dissected the mechanism of USP19 in IRF4 stabilization and found that USP19 overexpression impaired the IRF4–p62 association (Supplementary Fig. S3h). Likewise, in BM cells, we also detected the endogenous association of p62 and IRF4, and found that *Usp19* deficiency significantly enhanced the association between p62 and IRF4 (Fig. 4f). Finally, we found that USP19 could not further stabilize the IRF4 protein in *p62*-deficient

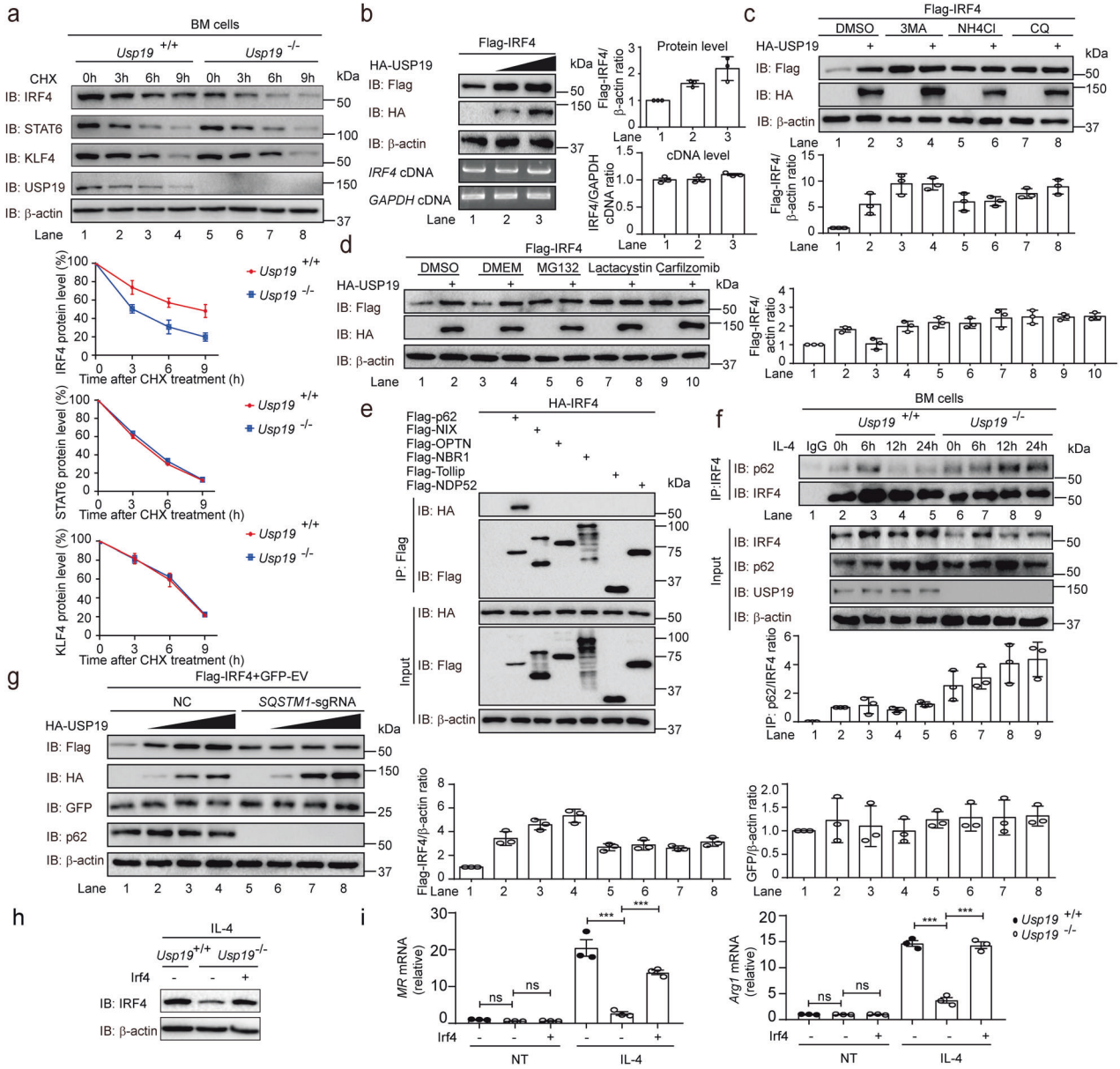

Fig. 4 USP19 prevents interferon regulatory factor 4 (IRF4) from p62-dependent autophagic degradation. **a** Wild-type (WT) or *Usp19*$^{-/-}$ BM cells were treated with cycloheximide (CHX; 100 μg/mL) at the indicated time points. Cell lysates were then collected for immunoblotting (upper). Quantification of the protein levels of IRF4, signal transducer and activator of transcription 6 (STAT6), and Kruppel-like factor 4 (KLF4; lower). **b** Human embryonic kidney (HEK) 293T-NLRP3 cells were transfected with plasmid for Flag-IRF4 and increasing doses of HA-USP19 for 24 h. Cell lysates were collected for immunoblot analysis (left top). The results of RT-PCR analysis of IRF4 cDNA are shown (left down); *GAPDH* cDNA served as a loading control. Quantification of the protein or cDNA levels of Flag-IRF4 (right). **c** HEK293T-NLRP3 cells were transfected with plasmid for Flag-IRF4 with or without plasmid for HA-USP19. Then, cells were treated with DMSO (vehicle), 3-methyladenine (3-MA; 10 mM), NH_4Cl (20 mM), or chloroquine (CQ; 50 μM) for 8 h. Cell lysates were collected for immunoblot analysis (upper). Quantification of the protein levels of Flag-IRF4 (lower). **d** HEK293T-NLRP3 cells were transfected with plasmid for Flag-IRF4 with or without plasmid for HA-USP19. Then, the cells were treated with lactacystin (5 μM), MG132 (10 μM) or carfilzomib (100 nM) for 6 h (left). Quantification of the protein levels of Flag-IRF4 (right). **e** Coimmunoprecipitation and immunoblot analysis of HEK293T cells transfected with HA-IRF4 with expression vectors for cargo receptors (Flag-p62, Flag-NIX, Flag-OPTN, Flag-NBR1, Flag-Tollip, and Flag-NDP52; input: 10%). **f** Extracts of WT or *Usp19*$^{-/-}$ BM cells treated with 20 ng/mL IL-4 for the indicated durations were subjected to immunoprecipitation with anti-IRF4 and immunoblotting with the indicated antibodies (input: 5%). Quantification of the interaction between p62 and IRF4 (lower). **g** HEK293T-NLRP3 cells were transfected with or without *SQSTM1*-sgRNA, after which cells were transfected with Flag-IRF4, GFP-empty vector (EV), and increasing doses of HA-USP19 plasmid (wedge), and cell lysates were collected for immunoblot analysis (left). Quantification of the protein levels of Flag-IRF4 (middle) and GFP (right). For all immunoblot data, similar results were obtained from three independent biological experiments. **h**, **i** Immunoblot analysis of extracts from BM cells transfected with mouse *Irf4* expression plasmid was carried out by using jetPEI reagent (PolyPlus) according to the manufacturer's instructions, after which the extracts were treated with IL-4 (20 ng/mL, 24 h) (**h**). Total RNA was harvested from the treated cells, and used for real-time PCR analysis to determine the expression of *MR* and *Arg1* (relative to *Gapdh*) (**i**)

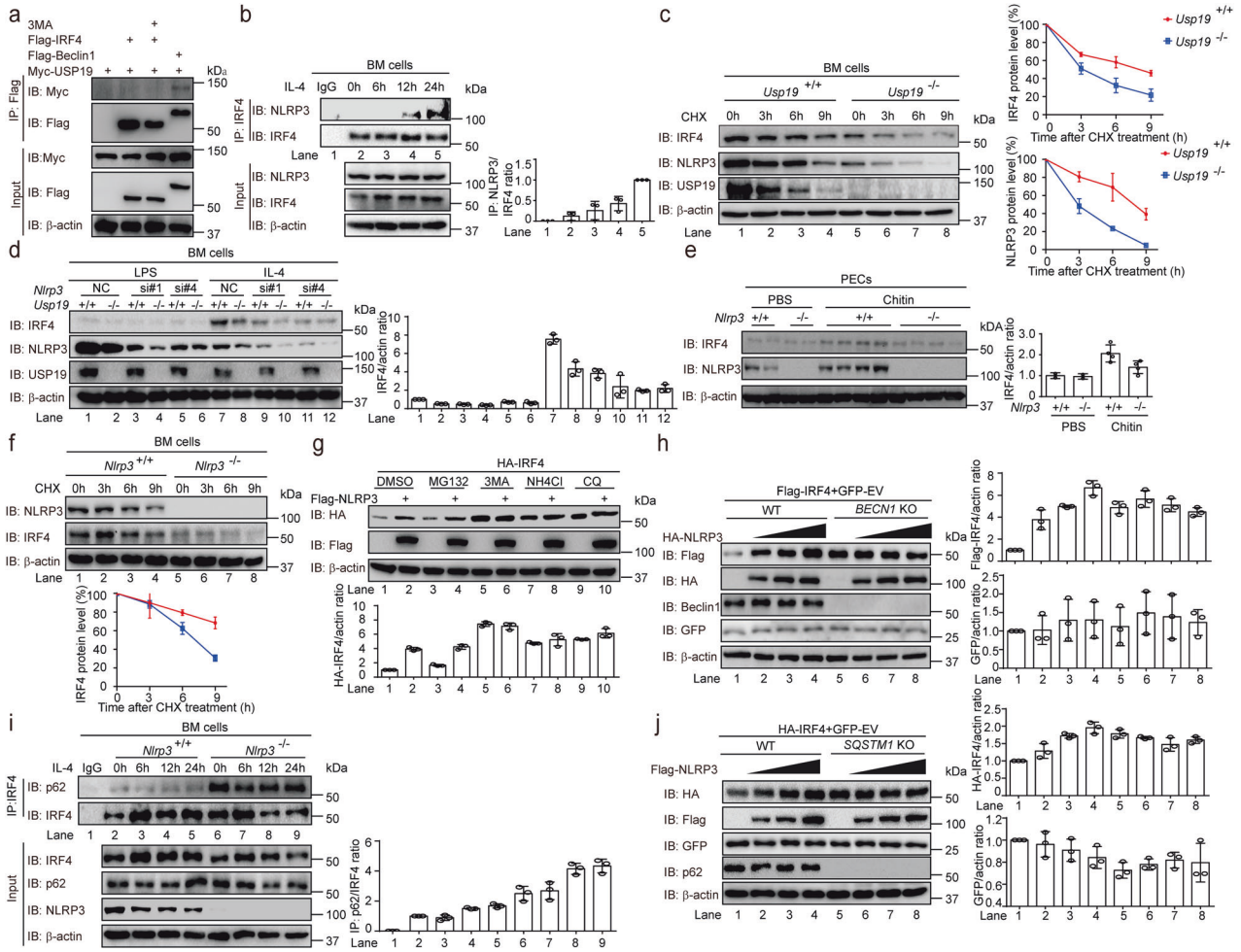

Fig. 5 USP19 stabilizes IRF4 via NLRP3. **a** HEK293T cells were transfected with Myc-USP19 and Flag-IRF4 (Beclin-1 acted as a positive control), and then treated with or without 3-MA (10 mM) for 8 h. Cell extracts were collected for immunoprecipitation with anti-Flag beads, followed by immunoblot analysis with anti-Myc antibody. **b** Extracts of BM cells treated with 20 ng/mL IL-4 for the indicated durations were subjected to immunoprecipitation with anti-IRF4 and immunoblot analysis with anti-NLRP3 (input: 5%). Quantification of the interaction between NLRP3 and IRF4 (right). **c** Wild-type (WT) or *Usp19*$^{-/-}$ BM cells were treated with CHX (100 μg/mL) at the indicated time points. Cell lysates were then collected for immunoblotting (left). Quantification of the protein levels of IRF4 and NLRP3 (right). **d** WT or *Usp19*$^{-/-}$ BM cells were transfected with control siRNA or *Nlrp3* siRNA for 48 h. Cells were stimulated with LPS (500 ng/mL, 3 h) or IL-4 (20 ng/mL, 4 h), and cell lysates were then collected for immunoblotting (left). Quantification of the protein levels of IRF4 (right). **e** WT or *Nlrp3*$^{-/-}$ mice were i.p. injected with chitin and incubated for 2 days. PECs were lysed and analyzed for the expression of NLRP3 and IRF4 by immunoblot analysis (left). For PBS-treated WT or *Nlrp3*$^{-/-}$ mice, each western blot included two samples per group. For chitin-challenged WT or *Nlrp3*$^{-/-}$ mice, each western blot included four samples per group. Quantification of the protein levels of IRF4 (right). **f** WT or *Nlrp3*$^{-/-}$ BM cells were treated with CHX (100 μg/mL) at the indicated time points. Cell lysates were then collected for immunoblotting (upper). Quantification of the protein levels of IRF4 (lower). **g** Immunoblot analysis of extracts of HEK293T cells transfected with plasmids for Flag-NLRP3 and HA-IRF4, and treated with MG132 (10 μM), 3-MA (10 mM), NH_4Cl (20 mM), or CQ (50 μM) for 8 h (upper). Quantification of the protein levels of HA-IRF4 (lower). **h** WT and *BECN1*-knockout (KO) HEK293T cells were transfected with Flag-IRF4, GFP-EV, and increasing doses of plasmid for HA-NLRP3 (wedge), and cell lysates were collected for immunoblot analysis (left). Quantification of the protein levels of Flag-IRF4 and GFP (right). **i** Extracts of WT or *Nlrp3*$^{-/-}$ BM cells treated with 20 ng/mL IL-4 for the indicated durations were subjected to immunoprecipitation with anti-IRF4, and immunoblot analysis with the indicated antibodies (input: 5%). Quantification of the interaction between p62 and IRF4 (right). **j** WT and *SQSTM1*-KO HEK293T cells were transfected with HA-IRF4 and GFP-EV, and increasing doses of plasmid for Flag-NLRP3 (wedge), and cell lysates were collected for immunoblot analysis (left). Quantification of the protein levels of HA-IRF4 and GFP (right). For all immunoblot data, similar results were obtained from three independent biological experiments

cells (Fig. 4g). In addition, we reexpressed mouse *Irf4* in *Usp19*$^{-/-}$ BM cells and observed that the reexpression of mouse *Irf4* restored IL-4-induced M2-like macrophage polarization in *Usp19*$^{-/-}$ BM cells (Fig. 4h, i). Collectively, these findings show that USP19 promotes M2-like macrophage polarization by preventing IRF4 from p62-mediated selective autophagic degradation.

USP19 stabilizes IRF4 via NLRP3

To investigate how USP19 prevents p62-mediated IRF4 degradation, we examined whether USP19 affects IRF4 stability through direct interaction. However, we did not detect an interaction between USP19 and IRF4, implying that the function of USP19 in stabilizing IRF4 is indirect (Fig. 5a). NLRP3 was recently reported to contribute to asthma through its cooperation with IRF4 in patients,[35] and M2-like macrophage polarization disorder is the main cause of asthma. We thus checked the function of NLRP3 in M2-like macrophage polarization and observed that NLRP3 deficiency decreased the proportion of M2-like macrophages, and reduced the recruitment of neutrophils in response to chitin in vivo

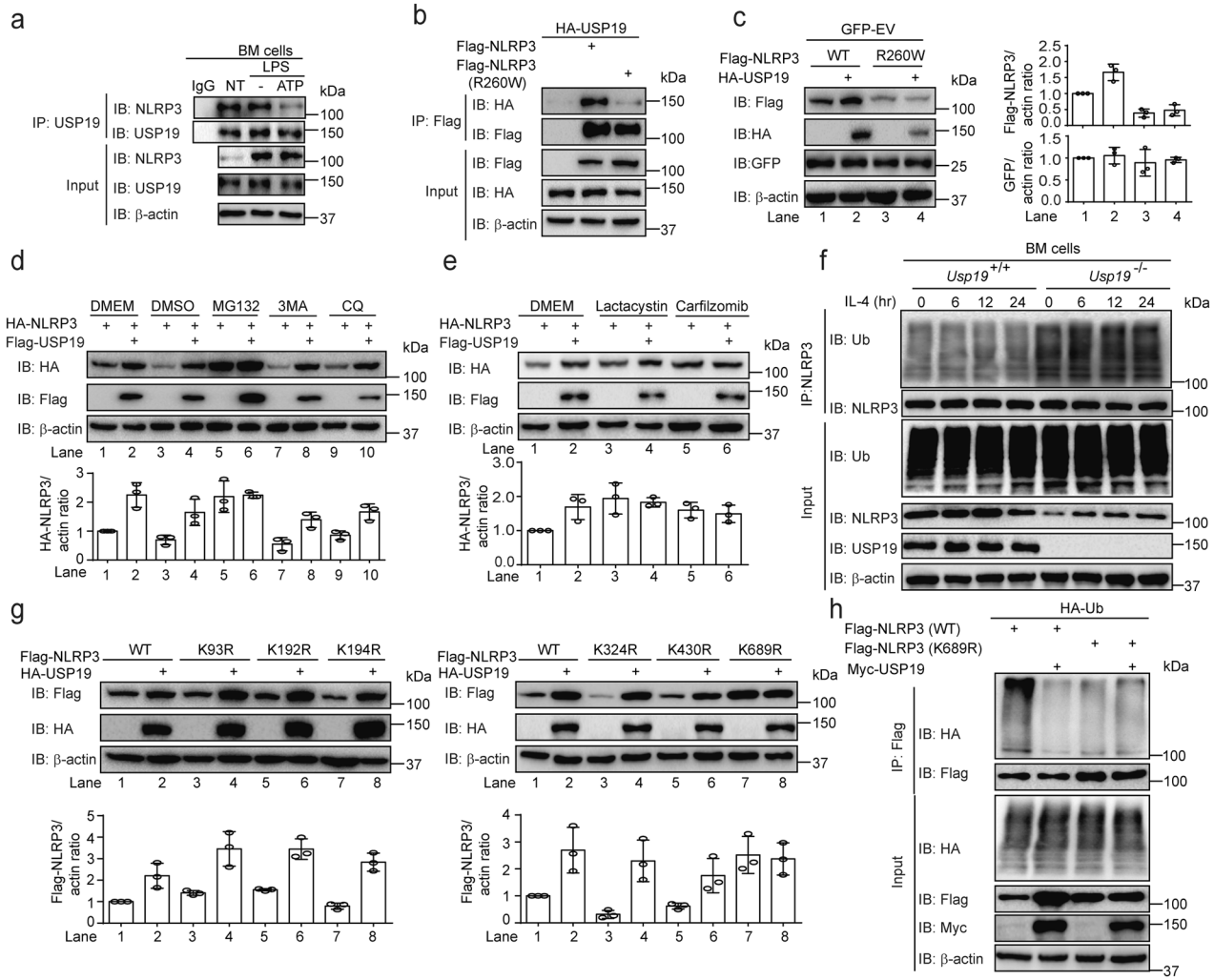

Fig. 6 USP19 stabilizes NLRP3 by cleaving its polyubiquitin chain at K689. **a** BM cells were primed with LPS (500 ng/mL, 3 h) and treated with ATP (5 mM, 6 h). Then, cell lysates were subjected to immunoprecipitation with anti-USP19 and immunoblot analysis with anti-NLRP3 (input: 5%). **b** HEK293T cells were transfected with HA-USP19 and Flag-NLRP3 or the NLRP3 R260W mutant. Cell lysates were immunoprecipitated with anti-Flag beads and immunoblotted with anti-HA (input: 10%). **c** HEK293T cells were transfected with Flag-NLRP3 or the NLRP3 R260W mutant with HA-USP19 and GFP-EV, respectively, and the extracts were analyzed by immunoblot analysis (left). Quantification of the protein levels of Flag-NLRP3 and GFP (right). **d** Immunoblot analysis of extracts of HEK293T cells transfected with plasmids for HA-NLRP3 and Flag-USP19 that were then treated with DMEM (vehicle), DMSO (vehicle), MG132 (10 μM), 3-MA (10 mM), or CQ (50 μM) for 8 h (upper). Quantification of the protein levels of HA-NLRP3 (lower). **e** Immunoblot analysis of extracts of HEK293T cells transfected with plasmids for HA-NLRP3 and Flag-USP19, and treated with DMEM (vehicle), lactacystin (5 μM), or carfilzomib (100 nM) for 6 h (upper). Quantification of the protein levels of HA-NLRP3 (lower). **f** Wild-type (WT) or *Usp19*$^{-/-}$ BMs were treated with IL-4 (20 ng/mL) at the indicated time points, after which the cell lysates were subjected to immunoprecipitation after sodium dodecyl sulfate (SDS) denaturation with anti-NLRP3 and immunoblotting with anti-ubiquitin (Ub; input: 5%). **g** HEK293T cells were transfected with HA-USP19 and Flag-NLRP3 WT or NLRP3 mutants, and the extracts were analyzed by immunoblot analysis (upper). Quantification of the protein levels of Flag-NLRP3 and its mutants (lower). **h** Immunoprecipitation and immunoblot analysis of HEK293T cells transfected with vectors for the expression of Flag-NLRP3 WT, or the indicated mutants and HA-tagged Ub in the presence of Myc-USP19 after SDS denaturation (input: 10%). For all immunoblot data, similar results were obtained from three independent biological experiments

(Supplementary Fig. S4a, b). Reexpression of mouse NLRP3 in *Nlrp3*$^{-/-}$ BM cells restored IL-4-induced M2-like macrophage polarization (Supplementary Fig. S4c). We further confirmed that IRF4 associates with NLRP3 after IL-4 stimulation in BM cells and that the N-terminus of IRF4 is critical for IRF4–NLRP3 association (Fig. 5b and Supplementary S4d). Interestingly, *Usp19* deficiency decreased the protein levels of both NLRP3 and IRF4 by affecting their degradation rates (Fig. 5c). In addition, we found that knockdown of *NLRP3* could significantly decrease IRF4 accumulation induced by USP19 (Fig. 5d). Collectively, these data indicate that NLRP3 might play an essential role in USP19-mediated IRF4 stabilization.

NLRP3 prevents the p62-mediated autophagic degradation of IRF4
Given that the protein levels of NLRP3 and IRF4 were similar in WT and *Usp19*$^{-/-}$ cells, we hypothesized that NLRP3 was responsible for IRF4 accumulation. We first collected chitin-treated WT and *Nlrp3*$^{-/-}$ PECs and found that *Nlrp3* deficiency abolished IRF4 accumulation (Fig. 5e). Ectopic NLRP3 expression strongly increased IRF4 accumulation (Supplementary Fig. S4e). Furthermore, we performed a CHX "chase" assay and demonstrated that *Nlrp3* deficiency accelerated the rate of endogenous IRF4 degradation (Fig. 5f). We next found that the autolysosome inhibitors 3-MA, CQ, and NH_4Cl alone stabilized IRF4 and that the addition of NLRP3 did not further stabilize IRF4. However, we did

not observe such effects upon treatment with the proteasome inhibitor MG132 (Fig. 5g). We further demonstrated that NLRP3 could not further increase IRF4 protein levels in *BECN1*-KO cells, in which autophagy was severely impaired (Fig. 5h). As IRF4 interacted with only p62 (Fig. 4d), we examined the interactions among IRF4, NLRP3, and p62. Our data showed that exogenous NLRP3 abolished the IRF4–p62 interaction (Supplementary Fig. S4f). This observation was further confirmed by the finding that *Nlrp3* deficiency significantly increased the IRF4–p62 association in response to IL-4 (Fig. 5i). Finally, we showed that NLRP3 could not further increase IRF4 protein levels in *SQSTM1*-KO HEK293T cells (Fig. 5j). Collectively, these data indicate that NLRP3 inhibits IRF4 degradation by blocking the IRF4–p62 interaction.

USP19 interacts with and stabilizes NLRP3

To further identify the molecular mechanism by which USP19 stabilizes the NLRP3 protein (Fig. 5c), we examined their direct interaction. In BM cells, endogenous USP19 and NLRP3 were directly associated, but their interaction was decreased by inflammasome activation (Fig. 6a). These data imply that NLRP3 incorporation into inflammasomes in M1-like macrophages diminishes its binding with USP19, so we hypothesize that NLRP3 that is not incorporated into inflammasomes might bind USP19 and promote M2-like macrophage polarization. Indeed, the NLRP3 R260W mutant, an active form of NLRP3 that directly triggers IL-1β secretion without stimulation,[36] had a decreased ability to bind USP19 compared to that of WT NLRP3 (Fig. 6b). Hence, USP19 could not stabilize the NLRP3 R260W mutant (Fig. 6c). In addition, by coexpressing NLRP3 and truncated NLRP3 domain constructs with USP19, we found that the LRR domain of NLRP3 mainly interacts with USP19 (Supplementary Fig. S5a). In addition, we also detected a weak association between USP19 and the NACHT domain of NLRP3, which contains R260. To determine how USP19 stabilizes the NLRP3 protein, we applied proteasome and autolysosome inhibitors, and found that USP19-mediated NLRP3 accumulation was abolished in the presence of the proteasome inhibitors MG132, lactacystin, and carfilzomib, but not the autolysosome inhibitors 3-MA or CQ (Fig. 6d, e). In addition, we performed a CHX "chase" assay and demonstrated that *Usp19* deficiency reduced the stability of endogenous NLRP3, but this phenotype could be attenuated by MG132 treatment (Supplementary Fig. S5b). These findings collectively suggest that USP19 directly binds NLRP3 that is not incorporated into the inflammasome and inhibits its proteasomal degradation.

USP19 cleaves the polyubiquitin chain of NLRP3 at lysine 689

We found that the catalytically inactive USP19 C506S/H1157A mutant failed to stabilize the NLRP3 protein (Supplementary Fig. S5c), suggesting that NLRP3 was stabilized through deubiquitination. We confirmed that USP19 deficiency significantly increased NLRP3 ubiquitination in response to IL-4 (Fig. 6f). Further experiments showed that USP19 specifically cleaved the K6-linked polyubiquitin chain of NLRP3, and a catalytically inactive mutant of USP19 failed to cleave the polyubiquitin chains of NLRP3 (Supplementary Fig. S5d, e). We next sought to identify which lysine (K) residues on NLRP3 are associated with this modification. Using computer-assisted algorithms (http://www.ubpred.org/cgi-bin/ubpred/ubpred.cgi), we identified six key ubiquitination sites in NLRP3 and substituted them with arginine (R) to create the K93R, K192R, K194R, K324R, K430R, and K689R NLRP3 mutants. We found that K689 in NLRP3 was required for USP19-mediated NLRP3 accumulation (Fig. 6g). Further assays confirmed that USP19 could not further deubiquitinate the NLRP3 K689R mutant (Fig. 6h). These results demonstrate that USP19 cleaves the polyubiquitin chain of NLRP3 at K689 and inhibits the proteasomal degradation of NLRP3.

DISCUSSION

Autophagy is an evolutionarily conserved degradation pathway under conditions of nutrient starvation or metabolic stress.[15] It is essential for cellular and tissue rejuvenation during various stress conditions. Increasing evidence indicates that autophagy is a selective process for the bulk degradation of long-lived proteins and organelles.[15] In selective autophagy, cargoes, such as proteins and organelles, are specifically recognized by various cargo receptors for selective degradation. For example, the cargo receptor p62 specifically mediates NEMO, AIM2, and ISG15-associated RIG-I for degradation, inhibiting NF-κB, AIM2 inflammasome, and type I IFN signaling, respectively.[15,37,38] However, the role of selective autophagy in macrophage polarization is not clear. Here, our current results show that the novel substrate IRF4, a critical transcription factor for macrophage polarization, can also interact with p62 for degradation. Importantly, the USP19-NLRP3 axis blocks IRF4 degradation by inhibiting the IRF4–p62 interaction, thereby promoting IRF4-mediated macrophage polarization.

Macrophage polarization is critical for immune homeostasis. Imbalance between M1-like/M2-like macrophages contributes to the pathogenesis of a variety of diseases, including obesity, fibrosis in organs, neuronal injuries, colorectal diseases, and cancer.[39,40] Previously, Jmjd3 and mTORC2 were reported to regulate M2-like macrophage polarization via IRF4.[7,9] Furthermore, increasing the evidence demonstrates that the deficiency of core autophagy genes or selective autophagy components drives IL-1β production, and promotes a proinflammatory myeloid cell phenotype associated with M1 cells both in vivo and in vitro.[41–43] Indeed, we found that deficient autophagy induced by the loss of *USP19* drove IL-1β production and ROS production, and promoted neutrophil recruitment. Instead, we did not find any significant changes in M1 macrophage polarization between WT and *Usp19*-deficient mice after alum treatment. We speculated that increased neutrophil recruitment in *Usp19*-deficient mice may act as a feedback mechanism to inhibit M1 macrophage polarization, since a high level of neutrophils was reported to promote the conversion of proinflammatory macrophages to proresolving macrophages.[44] In addition, *USP19*-deficient cells showed more cell death due to overactivated inflammasome signaling. The increased cell death of macrophages in *Usp19*-KO mice may counteract the positive effects of *Usp19*-KO on M1-like macrophage polarization, resulting in consistent M1-like macrophage polarization in USP19-deficient mice. Last, M1-like macrophages are not a unique cell type in inflammatory cytokine release. Inflammasome activation in intermediate M1/M2-polarized macrophages is intact.[45] Excluding M1-like macrophages, a high level of inflammasome activation in USP19-KO intermediate macrophages may contribute to IL-1β secretion and subsequent neutrophil recruitment without affecting M1 macrophage polarization. In addition, we demonstrated that USP19 prevented IRF4 degradation by inhibiting p62-mediated selective autophagy, and thus promoted M2-like macrophage polarization. Deficiency of USP19 in vivo led to the loss of the M2-like macrophage population, impaired eosinophil recruitment, and increased inflammatory cytokines in response to alum or chitin administration. Most likely, increased general autophagy and inhibition of selective autophagy for the degradation of certain proteins by USP19 will maximize the utilization of energy and maintain cellular homeostasis. Thus, USP19 promotes general autophagy for energy recycling and inhibits IRF4 degradation to maintain cell identity.

Although its best-known function is in inflammasome assembly, NLRP3 is also recognized to have inflammasome-independent roles. In the kidney epithelium, NLRP3 expression is increased in response to TGF-β and augments TGF-β signaling independent of inflammasome activation.[46] In the absence of ASC or caspase-1, NLRP3 acts as a nuclear DNA-binding transcription factor to promote TH2 differentiation, and contributes to allergic airway obstruction and melanoma tumor growth.[47] In addition, it was

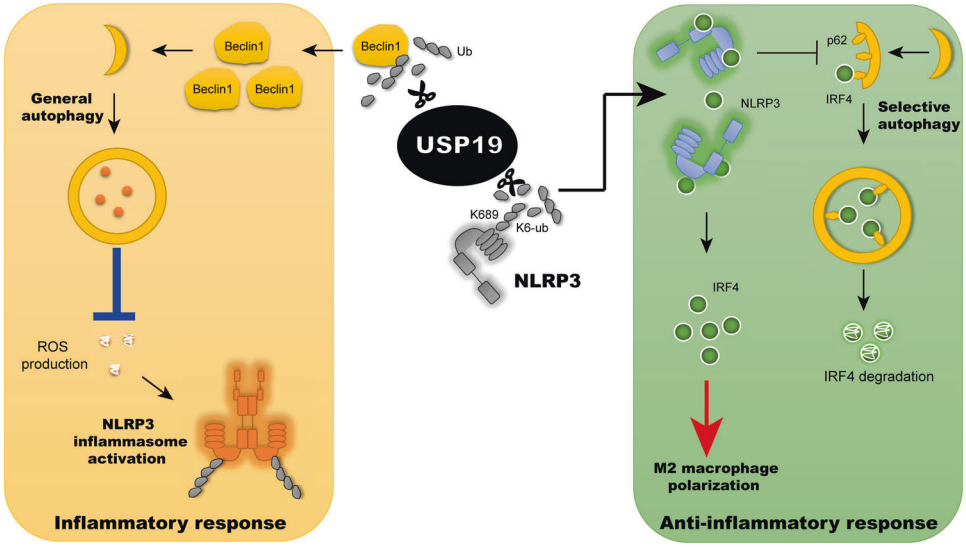

Fig. 7 A proposed working model to illustrate how the USP19-NLRP3 axis switches inflammatory and anti-inflammatory responses via autophagy. USP19 promotes autophagy by stabilizing Beclin-1 to mediate ROS clearance, leading to NLRP3 inflammasome inhibition. In contrast, USP19 also stabilizes NLRP3 by deubiquitination and targets NLRP3 to increase IRF4 accumulation through blocking the autophagic degradation of IRF4, enhancing M2-like macrophage polarization and anti-inflammatory responses

recently reported that NLRP3 promotes M2-like macrophage polarization and negatively regulates Treg differentiation.[35,48] Here, we have elucidated the mechanism by which NLRP3 promotes M2-like macrophage polarization by preventing p62-mediated selective IRF4 degradation via autophagy. We show that USP19 cleaves the polyubiquitin chain of NLRP3 at K689, and stabilizes NLRP3 expression. Although it is currently unknown whether pro- and anti-inflammatory NLRP3 differ in their K689 ubiquitination, this issue would be interesting to further investigate.

In summary, we propose a working model to demonstrate how USP19 shapes the function of NLRP3 in inflammation initiation and resolution (Fig. 7). In this model, on the one hand, USP19 promotes global autophagy, which clears ROS and downregulates NLRP3 inflammasome activation. On the other hand, USP19 stabilizes NLRP3 that is not incorporated in the inflammasome by removing its polyubiquitin chain on K689 and promotes the interaction of NLRP3 with IRF4, thereby preventing the p62-dependent selective autophagic degradation of IRF4. As macrophage polarization dysfunction is implicated in numerous human diseases, future developments that target USP19 may have therapeutic potential in inflammation-associated diseases.

MATERIALS AND METHODS

Mice

C57BL/6 *Usp19*$^{-/-}$ mice were generated by the CRISPR/Cas9 system. The pT7-3XFlaghCas9 plasmid was linearized with PmeI to synthesize Cas9 mRNA using the mMACHINE T7 ULTRA kit (Life Technologies). The pDR274 vector encoding a gRNA sequence (*Usp19* gRNA, 5′-GTGAACAGCCCTCTTGGCGCtgg-3′) was transcribed in vitro using the MEGAshortscript T7 kit (Life Technologies). The Cas9 mRNA and gRNAs were subsequently purified with the MEGAclear kit (Life Technologies), resuspended in RNase-free water, and quantified using a NanoDrop 1000. The mixture of Cas9 mRNA and gRNA was injected into 0.5-day zygotes of C57BL/6J mice. The injected zygotes were transplanted into the oviduct of 0.5-day pseudopregnant mothers 3 h after injection. CRISPR/Cas9 KO mice were bred with WT mice for more than three generations to avoid off-target effects. Mouse genotyping was performed by PCR and sequencing of tail snips with a mouse genotyping kit (KAPA Biosystems, KK7302) following the manufacturer's instructions. C57BL/6 *Nlrp3*$^{-/-}$ mice were kindly provided by Dr. Rongbin Zhou (University of Science and Technology of China). Animals were housed in a specific-pathogen free animal facility at Sun Yat-sen University. The Institutional Animal Care and Use Committee of Sun Yat-sen University, PRC, approved all the experimental protocols concerning the handling of mice.

Isolation of BM cells, PECs, and MEFs

Marrow was flushed from the bones, dissociated by pipetting, and cultured for 24 h in medium alone to obtain BM cells. The isolation of PECs and MEFs was performed as described previously.[49] To restore NLRP3 to *Nlrp3*$^{-/-}$ BM cells, NLRP3 was expressed through a lentiviral system in *Nlrp3*$^{-/-}$ BM cells by a standard transduction protocol, and the transduced cells were selected with puromycin (10 μg/mL). After one round of puromycin selection, the pool of cells was used for functional analyses.

Cells

HEK293T, BM cells, PECs, and MEFs were maintained in DMEM (HyClone) with 10% (vol/vol) fetal bovine serum (FBS; Gibco) and 1% L-glutamine (Gibco). THP-1 cells were cultured in RPMI 1640 medium (Gibco) supplemented with 10% (vol/vol) FBS and 1% L-glutamine. THP-1 cells were differentiated into macrophages by treatment with 100 ng/mL phorbol-12-myristate-13-acetate (Sigma) for 12 h and cultured with RPMI 1640. BMDMs or BMDCs were cultured for 6–8 days with 100 ng/mL macrophage colony-stimulating factor (PeproTech) or 20 ng/mL granulocyte macrophage colony-stimulating factor (PeproTech).[50] *BECN1*-KO and *SQSTM1*-KO HEK293T cells have been described previously.[15]

Reagents and antibodies

LPS and silica were purchased from Sigma. ATP, poly(dA:dT), MSU, alum, and CPPD were purchased from InvivoGen. IL-4 was purchased from PeproTech. Mito-TEMPO was purchased from Enzo. To induce starvation, cells were washed with PBS and incubated in EBSS (Gibco). Rapamycin, bafilomycin A1, CQ, and NH_4Cl were purchased from Sigma. Goat anti-rabbit (sc-2004), goat anti-mouse (sc-2005), mouse anti-goat (sc-2354), anti-ubiquitin (P4D1), anti-ASC (F-9), and anti-IRF4 (M-17) were purchased from Santa Cruz Biotechnology. Anti-NLRP3 (Cryo-z) was purchased from AdipoGen. Anti-caspase-1 (#2225), anti-IL-1β

(3A6), and anti-beclin-1 (#3738) were purchased from Cell Signaling Technology. Horseradish peroxidase (HRP)-anti-Flag (M2) (A8592) and anti-β-actin (A1978) were purchased from Sigma. HRP-anti-hemagglutinin (clone 3F10) and antic-Myc-HRP (11814150001) were purchased from Roche Applied Science. Anti-USP19 (YT4832) was purchased from Immunoway. Anti-p62 (18420-1-AP) was purchased from Proteintech. Alexa Fluor 647 rat Anti-CD206 (MR) and PE rat anti-mouse Siglec-F were purchased from BD Bioscience. PE anti-mouse F4/80 was purchased from Biolegend. Anti-mouse CD11b FITC and PE-Cy™7 anti-mouse Ly6G (Clone 1A8) were purchased from eBioscience.

Flow cytometry

PECs were labeled for 30 min at 4 °C using fluorochrome-conjugated monoclonal antibodies against mouse F4/80, CD11b, Ly6G, Siglec-F, and CD206 (MR; all antibodies are identified above.). Data were acquired using an LSR Fortessa cell analyzer (BD Biosciences).

Measurement of cytokines

The assay for cytokine measurement has been described previously.[51]

Cytotoxicity assay

Cell death was measured by a lactate dehydrogenase (LDH) assay using a CytoTox 96 Non-Radioactive Cytotoxicity Assay kit (Promega) and determined as follows:

% Cytotoxicity = 100 × (experimental LDH release − medium background)/(maximum LDH release control − medium background).

Fluorescence microscopy

The fluorescence microscopy assay has been described previously.[15]

Assay to measure active caspase-1 by fluorochrome-labeled inhibitors of caspase

The assay for active caspase-1 measurement has been described previously.[15]

Measurement of mitochondrial ROS

Peritoneal macrophages were stained with MitoSOX for 30 min in accordance with the manufacturer's instructions (Life Technologies). The cells were suspended in 1% FBS in PBS and then analyzed by flow cytometry with an LSR Fortessa cell analyzer.[52]

Immunoprecipitation, immunoblot analysis, and denatured ubiquitination assay

For immunoprecipitation, whole-cell extracts were prepared after transfection or stimulation with appropriate ligands, and then incubated overnight with the appropriate antibodies plus anti-Flag anti-HA beads (Sigma) or protein A/G beads (Pierce). The beads were washed three to five times with low-salt lysis buffer, and immunoprecipitates were eluted with SDS loading buffer (Cell Signaling Technology) and resolved by SDS–PAGE. For the ubiquitination assay, the beads were washed with low-salt lysis buffer containing a low concentration of SDS (0.5%) to reduce the effect of coimmunoprecipitated proteins. Then, the immunoprecipitates were eluted with SDS loading buffer (Cell Signaling Technology) and resolved by SDS–PAGE. Proteins were transferred to polyvinylidene fluoride membranes (Bio-Rad) and further incubated with the appropriate antibodies. The LumiGlo chemiluminescent substrate system (KPL) was used for protein detection.

Supernatant precipitation

The culture medium was changed to Opti-MEM without FBS before cells were stimulated with LPS or LPS plus inflammasome stimuli. The supernatants were harvested by centrifugation at 800 × *g* for 5 min and precipitated. An equal volume of methanol and a 0.25 volume of chloroform were added, and the mixtures were vortexed and then centrifuged for 15 min at 16,000 × *g*. The upper phase was discarded, and the same volume of methanol was added as before. The mixture was vortexed and then centrifuged for 15 min at 16,000 × *g*. The upper phase was discarded, and the protein pellets were dried at 55 °C. Pellets were mixed with 20 μL of 2× loading buffer and incubated at 95 °C for 5 min.

siRNA transfection

Chemically synthesized 21-nucleotide siRNA duplexes were obtained from TranSheep Bio (Shanghai, China) and transfected using Lipofectamine RNAiMAX (Invitrogen, Carlsbad, Calif) according to the manufacturer's instructions. The RNA oligonucleotides used in this study were as follows:

control siRNA, 5′-GUUAUCG CAACGUGUCACGUA-3′;
human *NLRP3* siRNA#1, 5′-GGCAGACCAUGUGGAUCUA-3′;
human *NLRP3* siRNA#2, 5′-AGAACUAGUUGACUAUAUA-3′;
human *USP19* siRNA#1, 5′-CGAGGACCUGAAUCGCAUUTT-3′;
human *USP19* siRNA#2, 5′-GGCGUGACAAGAUCAAUGATT-3′;
mouse *Nlrp3* siRNA#1, 5′-GGAUCUUUGCUGCGAUCAATT-3′; and
mouse *Nlrp3* siRNA#2, 5′-GGAUGAAC GUGUUCCAGAATT-3′.

Quantitative RT-PCR

Total RNA was extracted from the cells using TRIzol reagent (Invitrogen) according to the manufacturer's instructions. For RT-PCR analysis, cDNA was generated with HiScript® II Q RT SuperMix for qPCR (+gDNA wiper; Vazyme, Nanjing, China) and analyzed by quantitative real-time RT-PCR using the 2× RealStar SYBR Mixture (Genestar, Beijing, China). All data were normalized to *Gapdh* expression. Primer sequences were as follows:

mouse *Il-10*, sense: 5′- GCTCTTACTGACTGGCATGAG-3′,
anti-sense: 5′-CGCAGCTCTAGGAGCATGTG-3′;
mouse *MR*, sense: 5′-TACATGGAGATTGTCAACGTCAG-3′;
anti-sense: 5′-CCAGACCGACTATTGTCTTGC-3′;
mouse *Ym1*, sense: 5′-CAGGTCTGGCAATTCTTCTGAA-3′,
anti-sense: 5′-GTCTTGCTCATGTGTGTAAGTGA-3′;
mouse *Arg1*, sense: 5′-CTCCAAGC CAAAGTCCTTAGAG-3′,
anti-sense: 5′-GGAGCTGTCATTAGGGACATCA-3′;
mouse *Fizz1*, sense: 5′-CCAATCCAGCTAACTATCCCTCC-3′,
anti-sense: 5′-ACCC AGTAGCAGTCATCCCA-3′;
mouse *Nlrp3*, sense: 5′-ATTACCCGCCCGAGAAAGG-3′,
anti-sense: 5′-CATGAGTGTGGCTA GATCCAAG-3′;
mouse *Gapdh*, sense: 5′-GAAGGGCTCATGACCACAGT-3′, and
anti-sense: 5′-GGATGCAGGGATGATGTTCT-3′.

In vivo peritonitis

WT or *Usp19*$^{-/-}$ mice (6–7 weeks old) were i.p. injected with 700 μg of alum for 12 h. Peritoneal cavities were washed with 4 ml of PBS. The peritoneal fluids were harvested and concentrated for ELISA analysis, and PECs were analyzed by FACS.[19]

Chitin administration

Chitin (Sigma) was washed three times in PBS and then sonicated with a UR-20P device (Tomy) for 30 min on ice. After filtration with 100 μm cell strainers, the chitin was diluted in 50 ml of PBS. Approximately 800 ng of chitin was i.p. injected, and PECs were collected at 2 days after administration for FACS.[7]

Statistical analyses

Data are represented as the mean ± SD where indicated, and Student's *t* test was used for all statistical analyses with GraphPad Prism 5 software. Differences between groups were considered significant when the *P* value was <0.05.

ACKNOWLEDGEMENTS

This work was supported by the National Key Research and Development Project (2020YFA0908700) and the National Natural Science Foundation of China (31870862 and 31700760).

AUTHOR CONTRIBUTIONS

T.L., L.W., and P.L. performed the experiments and analyzed the results. X.W., Y.L., J.C., Y.S., D.W., Z.W., Z.G., and X.X. provided technical help. J.C. and J.H. initiated and designed the project, and directed the research. T.L., S.B., and J.C. wrote the manuscript.

ADDITIONAL INFORMATION

The online version of this article (https://doi.org/10.1038/s41423-020-00567-7) contains supplementary material.

Competing interests: The authors declare no competing interests.

REFERENCES

1. Saha, S., Shalova, I. N. & Biswas, S. K. Metabolic regulation of macrophage phenotype and function. *Immunol. Rev.* **280**, 102–111 (2017).
2. Murray, P. J. Macrophage polarization. *Annu. Rev. Physiol.* **79**, 541–566 (2017).
3. Kimura, T. et al. Polarization of M2 macrophages requires Lamtor1 that integrates cytokine and amino-acid signals. *Nat. Commun.* **7**, 13130 (2016).
4. Rathinam, V. A. et al. TRIF licenses caspase-11-dependent NLRP3 inflammasome activation by gram-negative bacteria. *Cell* **150**, 606–619 (2012).
5. Hwang, I. et al. Non-transcriptional regulation of NLRP3 inflammasome signaling by IL-4. *Immunol. Cell Biol.* **93**, 591–599 (2015).
6. Liao, X. et al. Kruppel-like factor 4 regulates macrophage polarization. *J. Clin. Investig.* **121**, 2736–2749 (2011).
7. Satoh, T. et al. The Jmjd3-Irf4 axis regulates M2 macrophage polarization and host responses against helminth infection. *Nat. Immunol.* **11**, 936–944 (2010).
8. Byles, V. et al. The TSC-mTOR pathway regulates macrophage polarization. *Nat. Commun.* **4**, 2834 (2013).
9. Huang, S. C. et al. Metabolic reprogramming mediated by the mTORC2-IRF4 signaling axis is essential for macrophage alternative activation. *Immunity* **45**, 817–830 (2016).
10. Lee, J. G., Kim, W., Gygi, S. & Ye, Y. Characterization of the deubiquitinating activity of USP19 and its role in endoplasmic reticulum-associated degradation. *J. Biol. Chem.* **289**, 3510–3517 (2014).
11. Wu, M. et al. USP19 deubiquitinates HDAC1/2 to regulate DNA damage repair and control chromosomal stability. *Oncotarget* **8**, 2197–2208 (2017).
12. Wu, X. et al. Regulation of TRIF-mediated innate immune response by K27-linked polyubiquitination and deubiquitination. *Nat. Commun.* **10**, 4115 (2019).
13. Lei, C. Q. et al. USP19 inhibits TNF-alpha- and IL-1beta-triggered NF-kappaB activation by deubiquitinating TAK1. *J. Immunol.* **203**, 259–268 (2019).
14. Jin, S. et al. USP19 modulates autophagy and antiviral immune responses by deubiquitinating Beclin-1. *EMBO J.* **35**, 866–880 (2016).
15. Liu, T. et al. TRIM11 suppresses AIM2 inflammasome by degrading AIM2 via p62-dependent selective autophagy. *Cell Rep.* **16**, 1988–2002 (2016).
16. Ren, K. & Torres, R. Role of interleukin-1beta during pain and inflammation. *Brain Res. Rev.* **60**, 57–64 (2009).
17. Guo, C. et al. Bile acids control inflammation and metabolic disorder through inhibition of NLRP3 Inflammasome. *Immunity* **45**, 802–816 (2016).
18. Kuroda, E. et al. Silica crystals and aluminum salts regulate the production of prostaglandin in macrophages via NALP3 inflammasome-independent mechanisms. *Immunity* **34**, 514–526 (2011).
19. Song, H. et al. The E3 ubiquitin ligase TRIM31 attenuates NLRP3 inflammasome activation by promoting proteasomal degradation of NLRP3. *Nat. Commun.* **7**, 13727 (2016).
20. Bal, S. M. et al. IL-1beta, IL-4 and IL-12 control the fate of group 2 innate lymphoid cells in human airway inflammation in the lungs. *Nat. Immunol.* **17**, 636–645 (2016).
21. Snelgrove, R. J. & Lloyd, C. M. An NLRP3, IL-1beta, neutrophil axis in the respiratory tract leaves you breathless. *Am. J. Respir. Crit. Care Med.* **196**, 253–254 (2017).
22. Audish, D. et al. NLRP3/cryopyrin is necessary for interleukin-1beta (IL-1beta) release in response to hyaluronan, an endogenous trigger of inflammation in response to injury. *J. Biol. Chem.* **284**, 12762–12771 (2009).
23. Kang, M. J., Jo, S. G., Kim, D. J. & Park, J. H. NLRP3 inflammasome mediates interleukin-1β production in immune cells in response to *Acinetobacter baumannii* and contributes to pulmonary inflammation in mice. *Immunology* **150**, 495–505 (2017).
24. Michaelis, K. A. et al. The TLR7/8 agonist R848 remodels tumor and host responses to promote survival in pancreatic cancer. *Nat. Commun.* **10**, 4682 (2019).
25. Dziarski, R. & Gupta, D. Staphylococcus aureus peptidoglycan is a toll-like receptor 2 activator: a reevaluation. *Infect. Immun.* **73**, 5212–5216 (2005).
26. Wolf, A. J. et al. Hexokinase is an innate immune receptor for the detection of bacterial peptidoglycan. *Cell* **166**, 624–636 (2016).
27. Kanneganti, T. D. et al. Bacterial RNA and small antiviral compounds activate caspase-1 through cryopyrin/Nalp3. *Nature* **440**, 233–236 (2006).
28. Franklin, B. S., Latz, E. & Schmidt, F. I. The intra- and extracellular functions of ASC specks. *Immunol. Rev.* **281**, 74–87 (2018).
29. Liu, X. et al. Inflammasome-activated gasdermin D causes pyroptosis by forming membrane pores. *Nature* **535**, 153–158 (2016).
30. Gross, C. J. et al. K(+) efflux-independent NLRP3 inflammasome activation by small molecules targeting mitochondria. *Immunity* **45**, 761–773 (2016).
31. Nakahira, K. et al. Autophagy proteins regulate innate immune responses by inhibiting the release of mitochondrial DNA mediated by the NALP3 inflammasome. *Nat. Immunol.* **12**, 222–230 (2011).
32. Cui, J., Jin, S. & Wang, R. F. The BECN1-USP19 axis plays a role in the crosstalk between autophagy and antiviral immune responses. *Autophagy* **12**, 1210–1211 (2016).
33. Motran, C. C. et al. Helminth infections: recognition and modulation of the immune response by innate immune cells. *Front. Immunol.* **9**, 664 (2018).
34. Reese, T. A. et al. Chitin induces accumulation in tissue of innate immune cells associated with allergy. *Nature* **447**, 92–96 (2007).
35. Liu, Y. et al. NLRP3 regulates macrophage M2 polarization through up-regulation of IL-4 in asthma. *Biochem. J.* **475**, 1995–2008 (2018).
36. Dowds, T. A., Masumoto, J., Zhu, L., Inohara, N. & Nunez, G. Cryopyrin-induced interleukin 1beta secretion in monocytic cells: enhanced activity of disease-associated mutants and requirement for ASC. *J. Biol. Chem.* **279**, 21924–21928 (2004).
37. Zhang, Y. et al. ANGPTL8 negatively regulates NF-kappaB activation by facilitating selective autophagic degradation of IKKgamma. *Nat. Commun.* **8**, 2164 (2017).
38. Du, Y. et al. LRRC25 inhibits type I IFN signaling by targeting ISG15-associated RIG-I for autophagic degradation. *EMBO J.* **37**, 351–366 (2018).
39. Ding, N. et al. Physalin D regulates macrophage M1/M2 polarization via the STAT1/6 pathway. *J. Cell. Physiol.* **234**, 8788–8796 (2019).
40. Koh, Y. C., Yang, G., Lai, C. S., Weerawatanakorn, M. & Pan, M. H. Chemopreventive effects of phytochemicals and medicines on M1/M2 polarized macrophage role in inflammation-related diseases. *Int. J. Mol. Sci.* **19**, 2208 (2018).
41. Saitoh, T. et al. Loss of the autophagy protein Atg16L1 enhances endotoxin-induced IL-1beta production. *Nature* **456**, 264–268 (2008).
42. Hubbard-Lucey, V. M. et al. Autophagy gene Atg16L1 prevents lethal T cell alloreactivity mediated by dendritic cells. *Immunity* **41**, 579–591 (2014).
43. Wang, Y. T. et al. Select autophagy genes maintain quiescence of tissue-resident macrophages and increase susceptibility to Listeria monocytogenes. *Nat. Microbiol.* **5**, 272–281 (2020).
44. Yang, W. et al. Neutrophils promote the development of reparative macrophages mediated by ROS to orchestrate liver repair. *Nat. Commun.* **10**, 1076 (2019).
45. Pelegrin, P. & Surprenant, A. Dynamics of macrophage polarization reveal new mechanism to inhibit IL-1beta release through pyrophosphates. *EMBO J.* **28**, 2114–2127 (2009).
46. Wang, W. et al. Inflammasome-independent NLRP3 augments TGF-beta signaling in kidney epithelium. *J. Immunol.* **190**, 1239–1249 (2013).
47. Ting, J. P. & Harton, J. A. NLRP3 moonlights in TH2 polarization. *Nat. Immunol.* **16**, 794–796 (2015).
48. Park, S. H., Ham, S., Lee, A., Moller, A. & Kim, T. S. NLRP3 negatively regulates Treg differentiation through Kpna2-mediated nuclear translocation. *J. Biol. Chem.* **294**, 17951–17961 (2019).
49. Chen, M. et al. TRIM14 inhibits cGAS degradation mediated by selective autophagy receptor p62 to promote innate immune responses. *Mol. Cell* **64**, 105–119 (2016).
50. Conti, L. & Gessani, S. GM-CSF in the generation of dendritic cells from human blood monocyte precursors: recent advances. *Immunobiology* **213**, 859–870 (2008).
51. Zheng, Y. et al. Zika virus elicits inflammation to evade antiviral response by cleaving cGAS via NS1-caspase-1 axis. *EMBO J.* **37**, e99347 (2018).
52. Shi, H. et al. NLRP3 activation and mitosis are mutually exclusive events coordinated by NEK7, a new inflammasome component. *Nat. Immunol.* **17**, 250–258 (2016).